Available online at www.sciencedirect.com
SCIENCE DIRECT®
Surface Science 541 (2003) 113–127
SURFACE SCIENCE
www.elsevier.com/locate/susc

Thermally induced chemistry and electron-mediated processes of pyridine on (2 × 1) and modified Si(1 0 0) surfaces: evidence of electron-induced condensation oligomerization

Q. Li, K.T. Leung *

Department of Chemistry, University of Waterloo, 200 University Ave West, Waterloo, Ont., Canada N2L 3G1

Received 19 February 2003; accepted for publication 30 June 2003

Abstract

The room-temperature (RT) adsorption and surface reactions of pyridine on Si(1 0 0)2×1 have been investigated by thermal desorption spectrometry, low-energy electron diffraction, and Auger electron spectroscopy. In addition to molecular desorption, evidence of dissociation into smaller fragments, including C_2H_2 and atomic hydrogen, was also found upon thermal desorption of pyridine chemisorbed on Si(1 0 0)2×1 at RT. Other possible surface processes such as hydrogen abstraction, fragmentation and dissociative desorption have also been identified on Si(1 0 0)2×1 surfaces modified by sputtering, and pre- and post-exposure of molecular oxygen and of atomic hydrogen. Evidence of condensation oligomerization of pyridine at RT has been found on Si(1 0 0)2×1 upon irradiated by low-energy electrons and on an oxidized Si surface even without electron mediation.

Keywords: Thermal desorption spectroscopy; Auger electron spectroscopy; Chemisorption; Aromatics; Silicon; Solid–gas interfaces; Electron bombardment

1. Introduction

Organic semiconductors have attracted much recent attention because of their unique physical and electronic properties associated with many potential applications in the microelectronics industry [1–4]. The interactions of heterocyclic hydrocarbons, such as thiophene (C_4H_4S) and furan (C_4H_4O), with semiconductor surfaces are of practical importance to the development of highly ordered thin-film conducting polymers [5,6]. The conductivity of a polymer depends on the degree of conjugation in the π-bond backbone, and the chain alignment and extension [6]. Polymers are often generated electrochemically and made (semi) conducting upon doping. In such a process, the structure of the polymer film is usually ill-defined and highly disordered because it is difficult to control the factors that regulate the structure and organization of the polymer. Consequently, the conductivity of the resulting polymer is usually

* Corresponding author. Tel.: +1-519-888-4567x5826; fax: +1-519-746-0435.
E-mail address: tong@uwaterloo.ca (K.T. Leung).

0039-6028/$ - see front matter © 2003 Elsevier B.V. All rights reserved.
doi:10.1016/S0039-6028(03)00890-2

low. A viable approach to improve the ordering of conducting polymers is to pre-align the monomers or oligomers on a well-defined single-crystal surface before initiating polymerization. The two-dimensional periodicity of the surface can be used as a template to produce a highly ordered thin-film polymer. Silicon with its directional bonding and special electronic properties [7,8] is an ideal choice for use as a template [9,10]. In addition to thermally induced chemistry, different forms of radiation (ultraviolet light, low-energy electrons and/or ions) have also been used to mediate surface polymerization upon monomers adsorption. An improved understanding of the factors that govern the adsorption and reactivity of heterocyclic hydrocarbons on silicon surfaces with and without mediation by thermal or non-thermal irradiation is therefore of fundamental technological interest.

Pyridine (C_5H_5N) is one of the most common hetero-hexacyclic hydrocarbons, with a dipole moment of 2.215 D due largely to the lone-pair electrons on the N heteroatom [11]. Unlike the adsorption of pyridine on Si(1 1 1) surfaces that has been studied extensively [12–15], only a limited number of theoretical studies have been reported for pyridine on Si(1 0 0) [16,17]. Based on the photoemission result, Piancastelli et al. proposed that the adsorption of pyridine on Si(1 1 1)2×1 involves an interaction of the lone-pair electrons of the N heteroatom and, to a lesser extent, an out-of-plane π-bond interaction with the ring tilted from the Si surface [12]. However, a high-resolution electron energy loss spectroscopy (HREELS) investigation later showed that the adsorption mechanism involves the breakage of C–H bonds and the formation of Si–C bonds [13]. A scanning tunneling microscopy study by Yagi et al. suggested a dipole-dipole interaction between pyridine and the Si(1 1 1)7×7 surface, and the interaction is electrostatic and not chemical in nature [15]. An earlier low-energy electron diffraction (LEED) and thermal desorption spectrometry (TDS) study by our group showed that the N heteroatom appears to cause reduced adsorption of pyridine on the Si surface but enhanced surface reactivity, relative to benzene [14]. In the case of benzene (C_6H_6), a large number of experimental [18–24] and theoretical studies [17,20,25–29] have revealed that the chemisorption of this homocyclic aromatic compound on Si(1 0 0)2×1 follows the Diels–Alder cycloaddition mechanism, giving rise to a di-σ bonded, cyclohexadiene-like adsorption species. Although pyridine is isoelectronic with benzene with a similar ring structure, it is not clear whether a similar chemisorption mechanism would apply. After investigating an N-end-on adsorption state and two side-on adsorption states by means of density functional calculations, Lu et al. proposed that the most favorable adsorption geometry for pyridine on Si(1 0 0) is the N-end-on geometry [16]. In addition, rapid electron-induced dissociation of pyridine on Si(1 1 1)7×7 was also observed by our group [14]. It is unclear whether pyridine would exhibit similar adsorption behaviour and electron-mediated processes on the structurally different Si(1 0 0)2×1 surface.

In the present work, the surface chemistry of pyridine on Si(1 0 0)2×1 and related surfaces is investigated by using TDS, LEED, and Auger electron spectroscopy (AES), with the goal to determine the role of the N heteroatom on thermal and electron-mediated surface reactions. The results are compared with those of pyridine on Si(1 1 1) surfaces [12–15] and with other hexacycles (benzene [17–29] and toluene [30,31]) on Si(1 0 0).

2. Experimental details

The home-built ultra-high vacuum (UHV) system (with a base pressure of better than 5×10^{-11} Torr) and the experimental procedure for the TDS experiments using a differentially pumped 1–300 amu quadrupole mass spectrometer (QMS) have been described in detail elsewhere [31]. A 12.5×3.5 mm substrate was cut from a polished p-type boron-doped Si(1 0 0) wafer (0.4 mm thick) with a resistivity of 0.0080–0.0095 Ω cm. Details of the sample mounting arrangement and the setup for measuring the sample temperature have also been described in our earlier work [31]. For the present TDS experiments, a home-built programmable proportional-integral-differential temperature controller (based on the TMS320c50 microprocessor [32]) was used to control an AC current power supply to provide a linear heating rate of 2 K/s.

Before introduction into the UHV chamber, the Si sample was first pre-cleaned by using a typical RCA procedure [33] that involved soaking in a basic peroxide solution consisting of equal parts of H_2O_2 (30%) and NH_4OH (30%) in 5–20 parts of water. The sample was thoroughly outgassed at 850 K for 20 h until the chamber pressure recovered to 2×10^{-10} Torr. To prolong the repeated usage of the same Si sample (for up to 50 TDS experiments), we used a modified cleaning procedure. The near-surface carbon concentration was first reduced to an acceptable level as monitored by AES by repeated cycles of Ar sputtering (at a glancing angle) and low-temperature annealing (up to 850 K). The sample was then flash-annealed to 1500 K while maintaining the chamber pressure below 1×10^{-9} Torr. The resulting surface cleanliness was confirmed by a sharp 2×1 LEED pattern at RT and the lack of any detectable Auger features attributable to C, O and S. Although we believe that this procedure can produce a clean surface, it is not possible for us to evaluate the amount of surface defects that could be generated from one sample preparation to the next. This small variation in the initial surface condition (estimated to be less than 20%) may in turn affect the absolute intensities of the TDS profiles.

The chemicals, pyridine (99.9 + % purity) and d_5-pyridine (99.5% D atom purity), used in the present study were obtained commercially from Aldrich and Cambridge Isotope Laboratories, respectively, and were degassed by repeated freeze-pump-thaw cycles prior to use. Sample dosing was performed by back-filling the sample preparation chamber to an appropriate pressure (as monitored by an uncalibrated ionization gauge) using a precision leak valve. All exposures (in units of Langmuir ($1\ \mathrm{L}=10^{-6}$ Torr s)) were performed at RT unless stated otherwise.

3. Results and discussion

3.1. Room-temperature adsorption of pyridine on Si(100)2 × 1

AES was used to study pyridine adsorption on Si(1 0 0)2×1 at RT. Fig. 1 compares the relative carbon concentration, as indicated by the peak-to-peak ratio of the C(KLL) Auger peak at 272 eV to the Si(LVV) Auger peak at 92 eV, as a function of RT exposure for pyridine and benzene on Si(1 0 0)2×1. The ratio appears to level off to its maximum value at a pyridine (benzene) exposure of 8 L (2 L), which indicates completion of adsorption of the first monolayer (ML). The saturation coverage for benzene has been estimated to be 0.27 ML by Taguchi et al. [18]. From the ratios of saturation for pyridine (10.2%) and benzene (8.0%) and after taking into account the numbers of carbon atoms in pyridine (5) and benzene (6), we determine the saturation coverage for pyridine to be 0.41 ML. The adsorption of pyridine on Si(1 0 0)2×1 is therefore over 50% higher than that

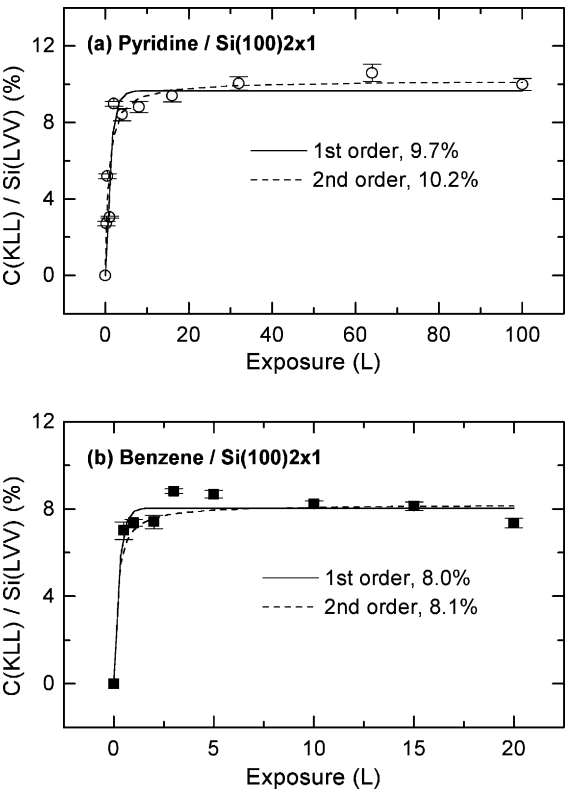

Fig. 1. Relative carbon moiety as reflected by the peak-to-peak intensity ratio for the C(KLL) to Si(LVV) Auger transitions as a function of room-temperature exposure of (a) d_5-pyridine and (b) benzene to Si(1 0 0)2×1. The experimental data are compared with fitted curves based on the first-order and second-order adsorption kinetic equations.

of benzene, which corresponds approximately to four d_5-pyridine molecules for every five Si dimers on the 2×1 surface. Furthermore, we have fitted the experimental data according to the following equations derived from first-order and second-order adsorption kinetics [34]:

$$\theta = \theta_0(1 - e^{-k_1\Lambda}) \quad \text{for first-order adsorption; and} \tag{1}$$

$$\theta = \theta_0 \frac{k_2\Lambda}{1 + k_2\Lambda} \quad \text{for second-order adsorption;} \tag{2}$$

where θ is the coverage and Λ is the exposure in L. The fitting parameters are the saturation coverage θ_0 and the adsorption rate constants k_1 and k_2. As shown in Fig. 1, the amount of adsorbed pyridine on the surface evidently follows a second-order kinetics in term of the fraction of unoccupied sites, which suggests that the adsorption of pyridine is a more complicated process (relative to benzene) possibly involving hydrogen abstraction and/or fragmentation at RT. For benzene on Si(1 0 0)2×1, the saturation coverage was found to be insensitive to the order of the adsorption kinetics, which has been shown to be first-order by Taguchi et al. [18] but could not be determined with our data set.

Fig. 2 shows the TDS profiles of mass 84 and mass 4 (corresponding to molecular and D_2 desorption, respectively) obtained at different RT exposures of d_5-pyridine on Si(1 0 0)2×1. It should be noted that deuterated pyridine was used in the present TDS study in order to avoid the large H_2 background commonly found in stainless steel UHV chambers. In addition to the parent ion (mass 84), other fragments including $C_4D_4^+$ (mass 56) and $C_4D_3^+$ (mass 54) were also monitored during the TDS experiments. Since the relative intensities of the corresponding peaks were found to be in good accord with those found in the cracking pattern of d_5-pyridine [35], the detected mass fragments could be largely attributed to dissociation of molecularly desorbed d_5-pyridine in the ionizer of the QMS. For exposures less than 0.25 L, a single desorption peak at 520 K (α state) is observed (Fig. 2). With increasing exposure, a new desorption peak emerges

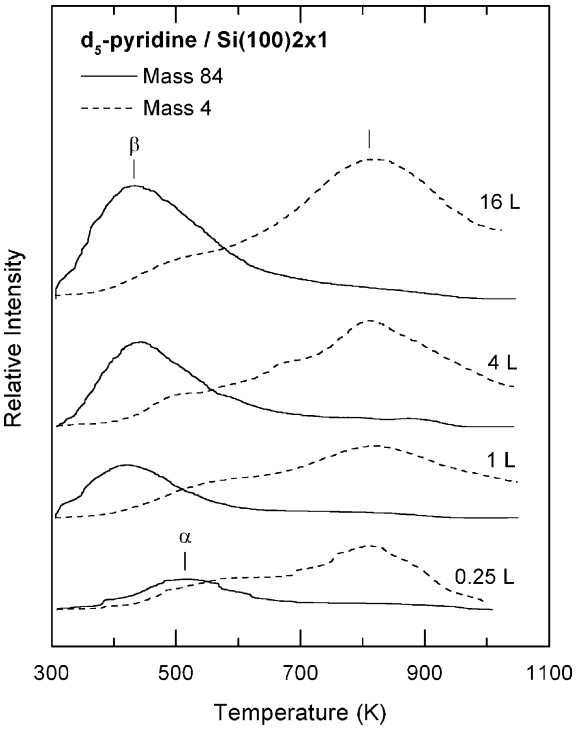

Fig. 2. Thermal desorption profiles of mass 84 (parent mass) and mass 4 (D_2) as a function of room-temperature exposure of d_5-pyridine to Si(1 0 0)2×1.

at 430 K (β state) along with the higher temperature peak (α state). The α state appears to reach saturation at a lower exposure than the β state. Within the absolute accuracy of our temperature measurement (±10 K), the desorption maxima of the α and β states remain essentially unchanged with increasing exposure, generally indicating first-order desorption kinetics [36]. The two molecular desorption maxima for pyridine/Si(1 0 0)2×1 are located very close in temperature to those of the corresponding peaks for benzene/Si(1 0 0)2×1 and for toluene/Si(1 0 0)2×1 [31]. The similarities found in the molecular desorption states indicate common chemisorption mechanisms for pyridine, benzene and toluene on Si(1 0 0)2×1, in particular involving the [2 + 2] and/or [4 + 2] cycloaddition reactions.

To identify the plausible adsorption geometries for the adsorption states of pyridine/Si(1 0 0)2×1,

we performed ab initio density functional calculations using Gaussian 98 [37] with hybrid functionals consisting of Becke's 3-parameter non-local exchange functional and the correlation functional of Lee-Yang-Parr (the so-called B3LYP method in Gaussian 98) [38]. Three different basis sets including STO-3G, 3-21G and 6-31G(d) have been used and found to give qualitatively similar adsorption geometries. A triple-dimer $Si_{21}H_{20}$ model was used to approximate the Si(1 0 0)2×1 surface, and three local energy minima have been found for C_5H_5N on this model surface. Fig. 3 shows the corresponding adsorption geometries obtained with the 6-31G(d) basis set. The first local minimum corresponds to an N-end-on atop configuration (Fig. 3a), with the N end of the pyridine molecule (and its ring in-plane with the Si dimer) datively bonded to the buckled-down Si atom of the dimer. The corresponding energy change ΔE with the zero-point energy correction for the adsorption of C_5H_5N on the $Si_{21}H_{20}$ cluster is calculated to be −32.3 kcal/mol (i.e., an exothermic process). The other two adsorption geometries follow the [4 + 2] cycloaddition mechanism, with the pyridine molecule di-σ bonded to the Si surface dimer via the C_2 and C_5 atoms (2,5 di-σ configuration, with ΔE of −20.7 kcal/mol, Fig. 3b) or via the N atom and the C_4 atom (1,4 di-σ configuration, with ΔE of −14.2 kcal/mol, Fig. 3c). The adsorption geometries obtained in the present work are found to be consistent with similar calculations by Lu et al. employing a smaller Si_9H_{12} cluster for modelling the Si surface [16]. For benzene adsorption on Si(1 0 0)2×1, we found from a similar calculation using the same $Si_{21}H_{20}$ cluster to represent the surface that the corresponding ΔE

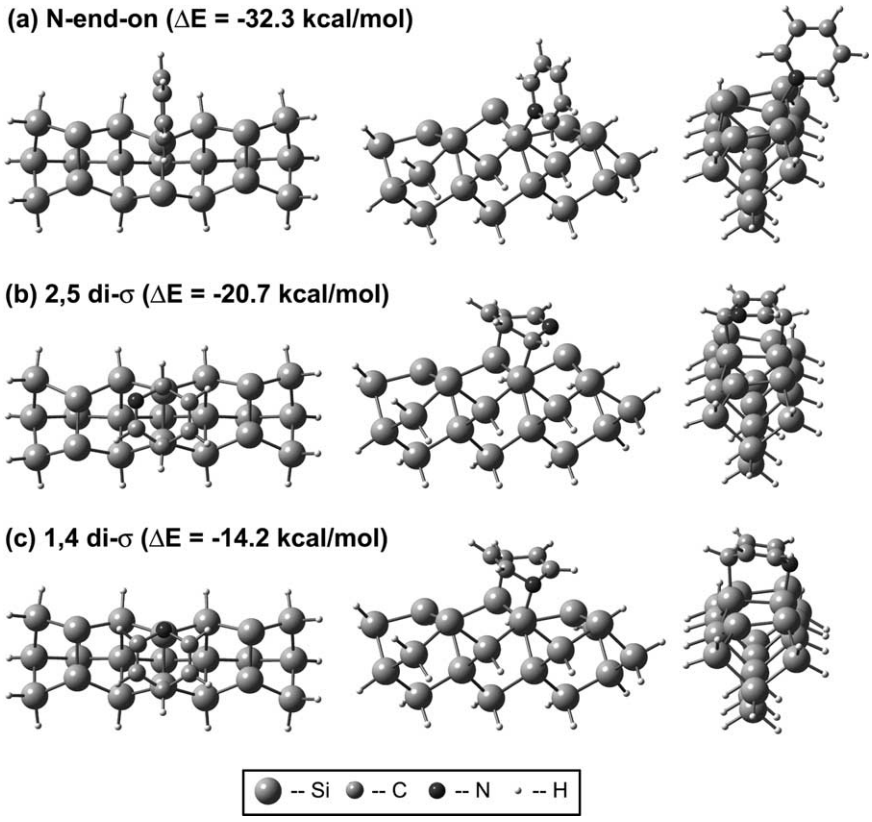

Fig. 3. Schematic diagrams of the adsorption geometries in three different perspectives and the corresponding adsorption energies ΔE obtained by a density functional calculation involving B3LYP/6-31G(d) for pyridine on the model surface of $Si_{21}H_{20}$.

for the [4 + 2] adsorption state that was found to desorb molecularly at 460 K [31] to be −16.2 kcal/mol, which is very close to that of the 1,4 di-σ state for pyridine/Si(1 0 0)2×1. The TDS peak at 430 K (Fig. 2) can therefore be attributed to the desorption of pyridine from the 1,4 di-σ adsorption geometry. From the relative values of the calculated ΔE values of the adsorption states, the TDS peak at 520 K (Fig. 2) can then be assigned to the 2,5 di-σ configuration. The more stable N-end-on atop adsorption state is believed to involve in other surface processes, as discussed later. The present calculation however has not considered and therefore could not be used to exclude the possibility of adsorption on defect sites and other adsorption geometries with even higher binding energies such as the double-dimer bridging configuration [23].

In addition to the molecular desorption profile, Fig. 2 also shows the mass-4 (D_2) TDS profiles with maxima at 810 K for RT exposures of d_5-pyridine on Si(1 0 0)2×1. The TDS profile can be attributed to recombinative molecular hydrogen desorption from monohydride with first-order kinetics [39,40]. The slightly elevated temperature of the desorption maximum from that of monohydride desorption (by 20 K) and the broad mass-4 profile with a long tail extending above 1000 K (Fig. 2) are related to the different sources of atomic hydrogen on the surface during the thermal desorption process. In particular, hydrogen abstraction of pyridine near or below its molecular desorption temperature could generate a comparable moiety of atomic hydrogen and other dissociated products, which could further release hydrogen mediated by the surface (both actively or via the availability of empty adsorption sites for H) at a temperature higher than the molecular desorption maximum. Furthermore, the shape of the observed mass-4 TDS profile (Fig. 2) can also be affected by the presence of surface hydrocarbon species, which could not only act as a source of H but also restrict the mobility of H during the thermal desorption process. Similar TDS behaviour for hydrogen desorption has also been reported by Taylor et al. for the adsorption and decomposition of acetylene on Si(1 0 0)2×1 [41]. In this case [41], the corresponding H_2 desorption peak was found to have an asymmetric shape with a maximum slightly higher by 10 K than the desorption maximum for monohydride and a long tail extending to 980 K, which has been proposed to arise from reaction-limited scission of C–H bonds followed by desorption of molecular hydrogen. As confirmed by HREELS [42], the dissociation of adsorbed acetylene via cleavage of the C–H bond is shown to occur over a wide temperature range of over 150 K near 750 K (i.e., below the C_2H_2 molecular desorption temperature). In contrast, the desorption maximum of molecular pyridine on Si(1 0 0)2×1 (near 430 K) is found to be considerably lower (Fig. 2). Furthermore, chemisorbed pyridine would not be expected to undergo thermal dissociation from the aforementioned di-σ adsorption geometries (Fig. 3), because the low adsorption energy ΔE of pyridine on Si(1 0 0) would enable pyridine to desorb before C–H bond activation. Hydrogen abstraction is therefore not likely to involve these di-σ states during annealing but other more stable states, such as the N-end-on atop adsorption state (Fig. 3a) and/or other intermediate states that could be populated during the thermal desorption process.

3.2. Electron irradiation of pyridine on Si(1 0 0)2 × 1

In our previous TDS work on irradiation of pyridine/Si(1 1 1)7×7 by a low-energy electron beam during a LEED experiment, a distinct dissociation reaction was observed at RT, which caused rapid conversion of the modified 7×7 LEED pattern to a 1×1 pattern within 60 s [14]. However, the LEED pattern for pyridine on Si(1 0 0)2×1 observed in the present work does not exhibit any discernible change and remains as 2×1 even after a prolonged period (70 min) of electron irradiation at ~80 eV beam energy and 10 μA beam current. In contrast, the corresponding thermal desorption experiments show markedly different TDS profiles, which underline the different thermal surface reactions. Fig. 4 compares the TDS profiles of the parent mass (mass 84), mass 28 and mass 4 for Si(1 0 0) saturated with 100 L of d_5-pyridine before and after electron irradiation at RT. Electron irradiation was performed on the Si sample (held at 80 V bias potential) for 30 min at

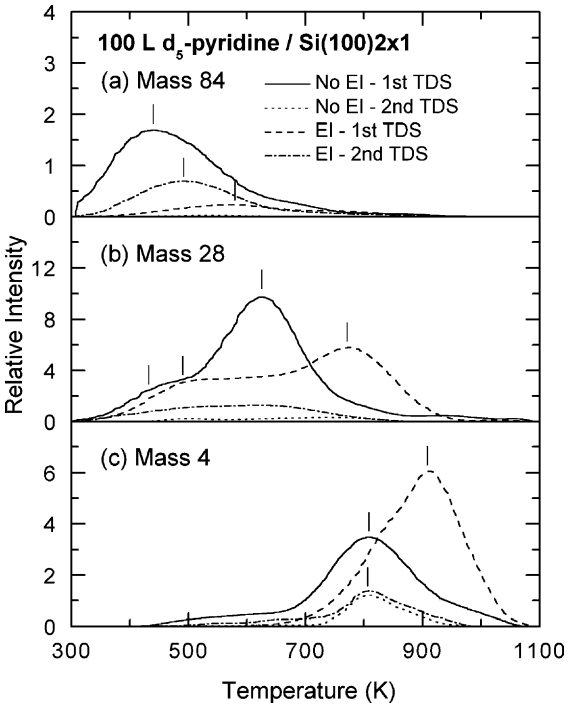

Fig. 4. Thermal desorption profiles for (a) mass 84 (molecular desorption) and dissociative products (b) mass 28 and (c) mass 4 for a 100 L room-temperature exposure of d_5-pyridine with and without electron irradiation at 200 μA and 80 eV for 30 min. The time difference between the first and second TDS experiments was 60 min.

200 μA with electrons thermionically emitted from a hot W filament positioned 5 cm away. Evidently, electron irradiation greatly diminishes the desorption of mass 84 (Fig. 4a), suggesting a significantly smaller moiety of molecularly adsorbed pyridine on the surface likely due to electron-induced desorption [43]. For the sample without electron irradiation, the weak mass-28 TDS peak at 430 K (Fig. 4b) coincides in temperature with the broad desorption feature of the parent mass (Fig. 4a) and can therefore be attributed to fragments of the molecularly desorbed pyridine created in the ionizer of the QMS. On the other hand, the strong mass-28 TDS peak at 630 K (Fig. 4b) does not have any obvious correlation with features in the TDS profile of the parent mass (Fig. 4a), and it should therefore be assigned to new desorbed products, including C_2D_2 and/or CND species resulting from direct dissociative desorption of d_5-pyridine. The contribution to mass 28 due to the cracking of desorbed C_2D_4 in the ionizer can be ruled out by the lack of corresponding TDS features of mass 30 (C_2D_3) or mass 32 (C_2D_4, normally with a desorption maximum near 550–580 K [44,45]). With electron irradiation, a new mass-28 TDS peak at 770 K emerges along with a mass-26 feature at the same temperature (not shown). These desorption features are characteristic of molecular desorption of C_2D_2 from Si(1 0 0)2×1 [41,42], and given that no such mass-28 feature is found for the sample without electron irradiation, new C_2D_2 and/or CND surface species must therefore be generated from electron-induced dissociation of the adsorbed pyridine at RT.

A considerably enhanced and broad mass-4 (D_2) TDS profile with a maximum shifted to a higher temperature (910 K) is observed upon electron irradiation (Fig. 4c). As with d_5-pyridine desorption without electron irradiation, the TDS feature at 810 K (appearing also as a shoulder on the lower temperature side of the broad TDS profile at 910 K) is attributed to recombinative desorption of D atoms from monohydride (Si-D) on the silicon surface, which follows first-order desorption kinetics (Fig. 2). The emergence of a strong feature at 910 K after electron irradiation suggests a different source for the adsorbed D atoms most likely coming from new deuterated hydrocarbon species. Since the TDS features for the monohydride species arising from the more common molecular fragments of d_5-pyridine usually occur at a lower temperature (e.g., 760 K for C_2D_4 [44] and 790–800 K for C_2D_2 [41]) on Si(1 0 0)2×1, the new contributing species are not due to adsorbed d_5-pyridine monomers or its smaller fragments but rather their oligomers. The presence of the strong D_2 TDS peak at 910 K therefore provides the first evidence of electron-induced condensation oligomeration of d_5-pyridine and/or related larger fragments on Si(1 0 0) at RT.

After completion of the TDS experiment for the electron-irradiated sample, the sample was allowed to cool for 60 min back to RT. A second TDS experiment was then performed on the same sample. Rather surprising results, particularly the rather strong molecular desorption of d_5-pyridine

(mass 84) at 500 K, have been observed for the second TDS run (Fig. 4a). Such phenomena have not been reported in the literature to the best of our knowledge. In general, there should not be any d_5-pyridine molecule left on Si(1 0 0) after annealing to over 1000 K in the first TDS experiment. Of the 60 min needed for cooling the sample naturally back to RT, for a period of at least 40 min the temperature of the sample was sufficiently high (above 400 K) for the desorption of d_5-pyridine. It is also unlikely that any re-adsorption of d_5-pyridine from the surrounding back onto the sample could occur in a vacuum better than 2×10^{-10} Torr. Furthermore, molecular desorption in the second TDS run was reproducible, though the observed intensity could vary by as much as 50%, causing the observed feature to be even higher than that found in the first TDS run (Fig. 4a). We have also performed a second TDS run on the sample without electron irradiation (Fig. 4) and found no molecular desorption nor features attributable to re-adsorption and/or experimental artefact.

To explain the results of the second TDS run, we hypothesize that the d_5-pyridine desorbed molecularly in the second TDS run originates from dissociation of the d_5-pyridine oligomers formed as a result of low-energy electron irradiation. While aliphatic hydrocarbons may tend to decompose and form carbides on surface upon annealing, polynuclear aromatic hydrocarbons prefer to cluster and form oligomers due to the strong unsaturated C–C bonding in the ring structure [46]. The dissociation of the oligomer is expected to occur at a low temperature (i.e., below 400 K), otherwise the dissociation products produced at a higher temperature would have desorbed during the cool-down period after the first TDS run. During the heating process (of the first TDS run), the interaction among the monomer units (of these oligomers) is stronger than the adsorbate–substrate interaction, and therefore the oligomers become loosely attached to the substrate surface [34]. Upon cooling, the adsorbate–substrate interaction becomes stronger than the adsorbate–adsorbate interaction of the monomers, causing oligomer dissociation. Furthermore, there should be a sufficient amount of active sites on the surface to facilitate the proposed oligomer dissociation, which are released by desorption of D_2 in the first TDS run. In corollary, the lack of unoccupied active sites also prevents oligomer dissociation during the first TDS run. A comparison of the second TDS run with the TDS without electron irradiation reveals a small shift in the molecular desorption peak from 430 to 500 K (Fig. 4a), which suggests that the d_5-pyridine monomers desorb primarily in the α state (Section 3.1) with the oligomer dissociation likely occurring at a lower temperature (350–400 K). Fig. 4c shows that the mass-4 TDS profile for the second TDS run resembles that without electron irradiation except for a lower intensity, which is consistent with the presence of a smaller moiety of monomers resulting from oligomer dissociation that leads to the hydrogen evolution. Similarly, Fig. 4b also shows that a greatly weakened TDS profile for mass 28 relative to that without electron irradiation, in good accord with our hypothesis.

3.3. Surface condition studies

Fig. 5 compares the TDS profiles for molecular desorption (mass 84) and dissociative products (mass 28 and mass 4) for the 2×1 and modified Si(1 0 0) surfaces saturated with d_5-pyridine. The amorphous Si (a-Si) surface was produced by ion sputtering in 4×10^{-5} Torr of Ar at 1 keV beam energy for 20 min, while the oxidized Si(1 0 0) surface was obtained by exposing a clean Si(1 0 0)2×1 surface with 100 L of O_2 at RT. The lack of any long-range order for both a-Si and oxidized Si surfaces was confirmed by the absence of a LEED pattern. With the sample temperature held near RT (280–300 K) by liquid-nitrogen cooling, the H-terminated Si(1 0 0) surface was prepared by exposing 3000 L of H_2 to a clean (2×1) surface with a hot W filament positioned 2 cm away, and the surface saturation of H atoms was confirmed by a sharp 1×1 LEED pattern [47].

The general TDS features for the a-Si surface can be qualitatively interpreted as the corresponding features for the Si(1 0 0)2×1 surface (Fig. 5). However, the overall desorption intensity for mass 84 on a-Si is found to be considerably lower than that for the 2×1 surface (Fig. 5a), which suggests that Ar sputtering appears to have re-

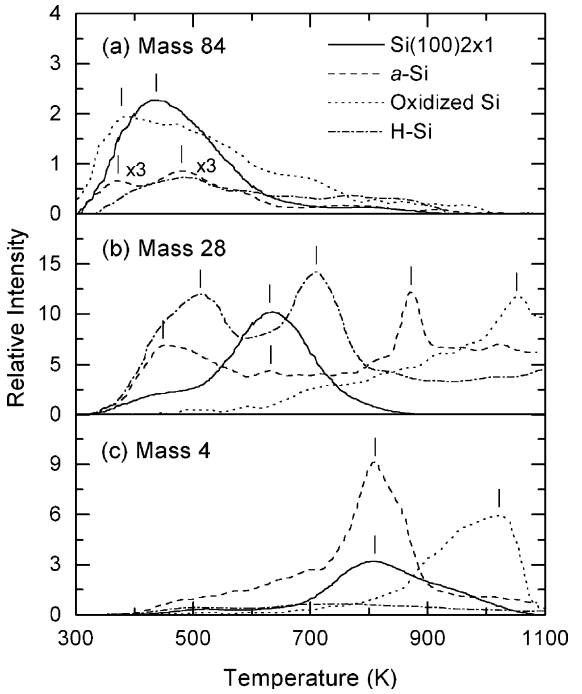

Fig. 5. Thermal desorption profiles for (a) mass 84, (b) mass 28 and (c) mass 4 for a saturation room-temperature exposure of d_5-pyridine to the 2×1, amorphous (a-), oxidized and H-terminated surfaces of Si(1 0 0).

duced the amount of adsorption sites compatible with di-σ bonding. Furthermore, the relative moiety of the α state for molecular desorption (at 510 K) appears to be higher than the β state (Fig. 2), which gives rise to the desorption maximum at 480 K in Fig. 5a. The relative changes in the moieties of these states for the a-Si surface therefore suggest that the presence of defect sites on the sputtered surface would favour adsorption in the α state. The feature at 370 K appears to correspond to a new desorption state for the a-Si surface. The weaker TDS structure of mass 28 at 630 K compared to that for the 2×1 surface (Fig. 5b) indicates a relatively small degree of dissociation upon RT adsorption of d_5-pyridine on the sputtered surface. The distinct mass-28 TDS peak at 870 K, which appears to accompany significant desorption of mass 40 at 880 K (corresponding to desorption of implanted Ar as a result of the sputtering process, not shown), could be attributed to dissociative desorption of fragments of hydrocarbon species from a fairly active surface. It should be noted that the strong desorption of mass 40 observed at 880 K correlates well with a very active Si surface with intense structural rearrangement at this temperature, which could cause the hydrocarbon remnants to undergo dissociative desorption. Except for the enhanced intensity, the single mass-4 TDS peak at 810 K for the a-Si surface is very similar to that for the 2×1 surface (Fig. 5c).

Fig. 6 compares the TDS profiles for molecular desorption (mass 84) and dissociative products (mass 28 and mass 4) for a 10 L RT exposure of d_5-pyridine to an a-Si surface before and after electron irradiation at 200 μA and 80 eV for 30 min. Evidently, exposing the sputtered Si surface to low-energy electrons does not appear to produce markedly different TDS features, except for the intensity. In particular, the intensity of the mass-84 TDS profile for the a-Si surface has been greatly

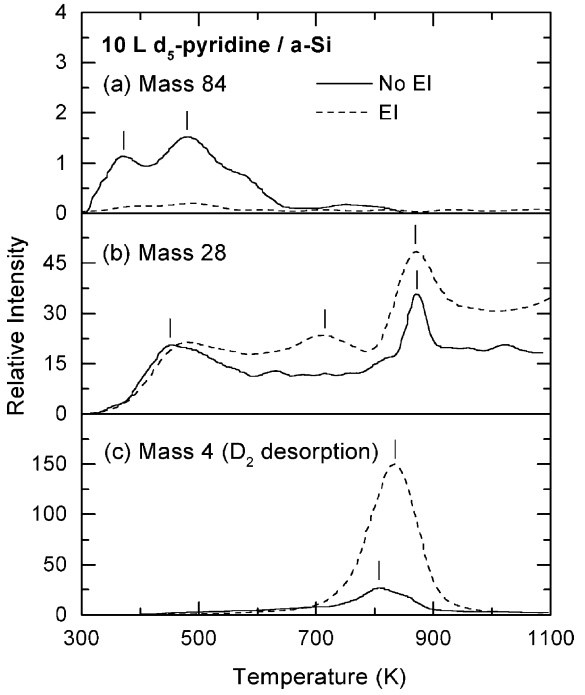

Fig. 6. Thermal desorption profiles for (a) mass 84, (b) mass 28 and (c) mass 4 for a 10 L room-temperature exposure of d_5-pyridine to an amorphous (a-)Si surface with and without electron irradiation at 200 μA and 80 eV for 30 min.

reduced by the electron irradiation, which again suggests electron-induced desorption of the molecularly adsorbed pyridine. On the other hand, the intensity of the mass-28 TDS profile particularly above 600 K has apparently been enhanced after electron irradiation, suggesting that there is a higher moiety of fragments that undergoes electron-induced dissociation on the amorphous surface. The mass-28 feature at 710 K (Fig. 4b) can be attributed, as for the case of the 2×1 surface, to C_2D_2 desorption [41]. Similar to the 2×1 surface, the mass-4 TDS peak is shifted to a higher temperature (i.e., from 810 to 840 K) but with a significantly enhanced intensity after electron irradiation. The apparent smaller shift in the desorption maximum to 840 K due to electron irradiation in the case of a-Si (Fig. 6c), relative to that for the 2×1 surface (910 K, Fig. 4c), could be due to defect sites.

Fig. 5 also shows the TDS profiles of mass 84, mass 28 and mass 4 for a 10 L RT exposure of d_5-pyridine on an oxidized Si(1 0 0) surface. The similarities in the TDS profiles of mass 84 below 600 K suggest that both the oxidized and (2×1) surfaces contain similar adsorption sites for pyridine (Fig. 5a). On the other hand, significant differences in the mass-28 and mass-4 TDS profiles between the 2×1 and oxidized surfaces are observed. In particular, the new desorption peak of mass 28 at ~1050 K (Fig. 5b) is found to exhibit a desorption maximum 30 K higher than that of the mass-4 desorption peak (Fig. 5c). The lack of the corresponding lower mass fragments, e.g., mass 26 (not shown), suggests that mass 28 is not due to desorption of C_2D_2 or CND fragments, but rather to associative desorption of CO. Since the adsorption energies of CO on Si(1 0 0)2×1 have been estimated to be −17–19 kcal/mol [48] and the desorption maximum for CO on Si(1 0 0) (at 180 K) [49] is markedly lower than the present TDS peak, other dissociation channels by which C readily combines with O on the oxidized surface to produce the desorbed CO could be activated (Fig. 5b) along with hydrogen evolution at such a high temperature (Fig. 5c). Of particular interest is the shift in temperature of the desorption maximum for mass 4 (D_2) on the oxidized surface by 210 K higher than that on the 2×1 surface (Fig. 5c). The strong mass-4 TDS peak at 1020 K can be attributed to recombinative desorption following plausible oligomer dissociation. The formation of oligomer has been proposed earlier in Section 3.2 as a plausible electron-induced process for pyridine on Si(1 0 0)2×1. The mechanism for such oligomer formation on the oxidized Si surface is however unclear but it may involve N–O interactions.

After the oxidized sample naturally cooled to RT in 60 min upon completion of the first TDS experiment, a second TDS run was performed and the corresponding profiles are shown in Fig. 7. Of special interest is the reappearance of mass 84 (molecular desorption) over its "normal" desorption temperature range (400–600 K) in the second TDS run (Fig. 7a), which is accompanied by notable mass-4 desorption with maximum at 810 K (Fig. 7c) and mass-28 desorption near 610 K (Fig. 7b). As with the case of the 2×1 surface (Fig. 5b), the mass-28 TDS feature at 610 K (Fig. 7b) can be

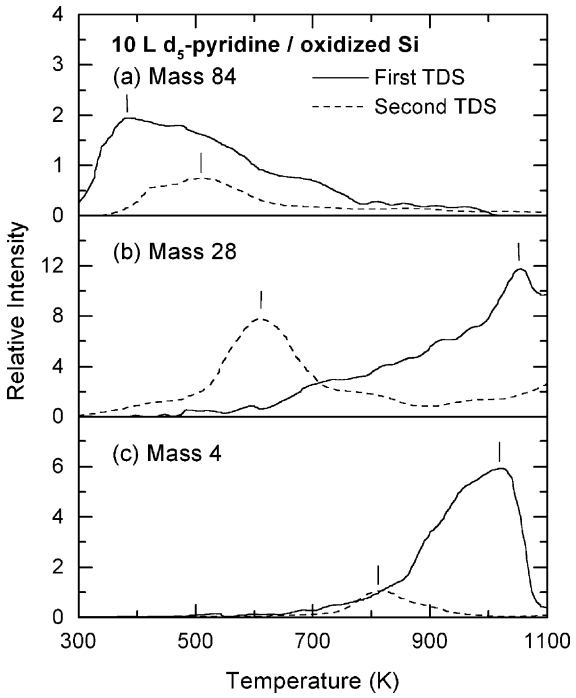

Fig. 7. Thermal desorption profiles for (a) mass 84, (b) mass 28 and (c) mass 4 for a 10 L room-temperature exposure of d_5-pyridine to an oxidized Si surface. The time difference between the first and second TDS experiments was 60 min.

attributed to NCD and C_2D_2 but not to C_2D_4 because no mass 30 (corresponding to C_2D_4) is found. The changes in these desorption profiles for the second TDS run are similar to those found earlier in Section 3.2, which further supports that condensation oligomerization could play an important role in the observed desorption behaviour of pyridine on the oxidized Si surface.

Fig. 5 also compares the TDS profiles of mass 84, mass 28 and mass 4 for a 10 L RT exposure of d_5-pyridine on a H-terminated Si(1 0 0) surface with other surface conditions. Like the a-Si sample, molecular desorption (mass 84) for the H-terminated Si(1 0 0) surface is found to be very weak (Fig. 5a). However, unlike the a-Si sample where an intense mass-4 desorption peak is observed at 810 K, the corresponding mass-4 desorption for the H-terminated Si(1 0 0) surface is found to be featureless, broad and weak (Fig. 5c). The weak mass-84 and mass-4 desorption features for the H-terminated sample would appear to suggest that pre-adsorbed H atoms have completely filled the active surface sites, hence preventing the adsorption of pyridine on Si(1 0 0)2×1. However, the strong mass-28 TDS structure with desorption maxima at 430, 520 and 710 K is found to be markedly different from that for Si(1 0 0)2×1 (630 K), a-Si (450, 630 and 870 K) and oxidized Si surface (1050 K), which indicates different pyridine dissociation pathways for producing mass 28 on the H-terminated Si(1 0 0) surface.

In order to investigate these perhaps more complex adsorption processes, TDS profiles of a more extended list of masses have been collected for a 10 L RT exposure of d_5-pyridine on the H-terminated Si(1 0 0) sample, shown in Fig. 8. Unlike the weak mass-4 desorption, two strong mass-2 TDS peaks at 680 and 790 K are found to correlate with the recombinative desorption of H_2 from the dihydride (β_2) and monohydride phases (β_1), respectively, of the H-terminated Si(1 0 0) surface [39,40] (Fig. 8). However, the presence of a weak mass-3 TDS peak at 800 K (near the desorption maximum of the β_1 state of H_2) indicates that part of the d_5-pyridine molecules adsorbed on the H-terminated surface undergoes dissociation and that the abstracted D atoms then recombine with the surface H atoms to form the desorbed

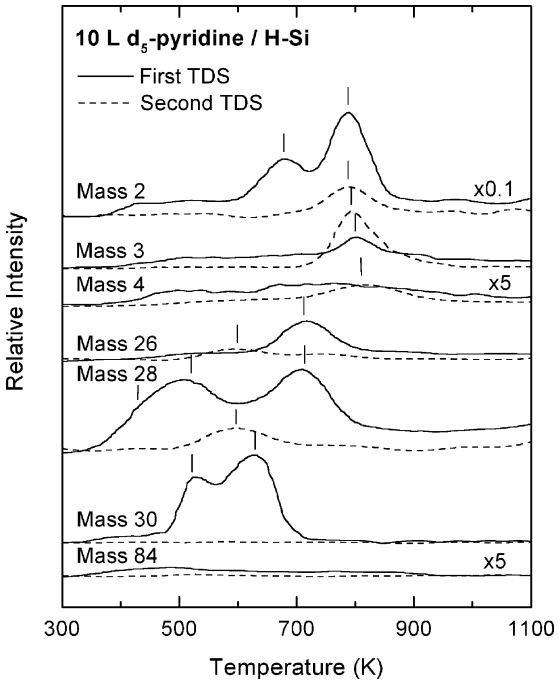

Fig. 8. Thermal desorption profiles of mass 2, 3, 4, 26, 28, 30, and 84 for a 10 L room-temperature exposure of d_5-pyridine to a H-terminated Si(1 0 0)2×1 surface. The time difference between the first and second TDS experiments was 60 min.

HD. Furthermore, in accord with an earlier study on the interaction of atomic H with adsorbed ethylene and acetylene on Si(1 0 0) [50], the TDS feature of mass 28 at 710 K that is accompanied by the mass-26 peak in the same temperature range can be attributed to desorption of C_2H_4 [50,51]. The mass-28 feature observed at a lower temperature (520 K) can be attributed predominantly to desorption of $C_2D_nH_{4-n}$ ($n = 0$–2) fragments [50,51], while the mass-30 features at 520 and 630 K can be assigned to desorption of $C_2D_2H_2$.

Fig. 8 also shows the results of a second TDS run for the d_5-pyridine/H-terminated Si(1 0 0) sample. As expected, the overall mass-2 desorption has been significantly reduced, with only the β_1 feature remaining. However, the TDS feature of mass 3 at 795 K (corresponding to recombinative desorption of HD) becomes considerably more intense in the second TDS run, which suggests that the majority of the D atoms abstracted from the

remaining hydrocarbon species after the first TDS run undergoes recombinative desorption with H atoms in the monohydride phase. In addition, the TDS profiles of both mass-28 and mass-26 in the second TDS run (Fig. 8) have evidently reverted back to those found for the Si(1 0 0)2×1 sample, with a single desorption feature near 600 K (Fig. 5b), suggesting dissociative desorption of C_2D_2 and/or NCD. Furthermore, the mass-30 TDS features at 520 and 630 K, along with the mass-28 features at 520 and 710 K and the mass-26 feature at 710 K, could not be observed in the second TDS run (Fig. 8). The lack of these desorption features in the second TDS run is consistent with the reduced moiety of H on the surface after the first TDS run. Unlike the earlier cases involving second TDS runs for electron-irradiated and oxidized samples, there is no evidence of oligomerization, which is consistent with our hypothesis that monomer adsorption is a required precondition.

3.4. Post-adsorption surface-mediated oxidation and hydrogenation reactions

Fig. 9 shows the TDS profiles of a 30 L post-exposure of O_2 to Si(1 0 0)2×1 saturated with 10 L of d_5-pyridine at RT. In particular, post-oxidation appears to reduce (mass 84) molecular desorption from the lower temperature β state (at 430 K) and (mass 4) D_2 evolution with desorption maximum at 810 K. Furthermore, essentially no desorption is observed for mass 30 upon post-oxidation (not shown), while desorption maxima for mass 28 (Fig. 9b) and mass 26 (not shown) are found to shift to a higher temperature (770 K) with O_2 post-exposure, which indicates that C_2D_2 is likely produced through the dissociation of d_5-pyridine. This shift in the mass 28 feature may be caused by surface interaction of dissociated fragments with coadsorbed O atoms, which produce an apparent stabilization effect. Unlike d_5-pyridine adsorption on the oxidized Si(1 0 0) surface (Section 3.3), the dramatic temperature increase in the mass-4 desorption maxima as a result of plausible oligomerization is not observed in the post-oxidation experiment.

In order to investigate the interaction of atomic hydrogen with pyridine adsorbed on Si(1 0 0)2×1,

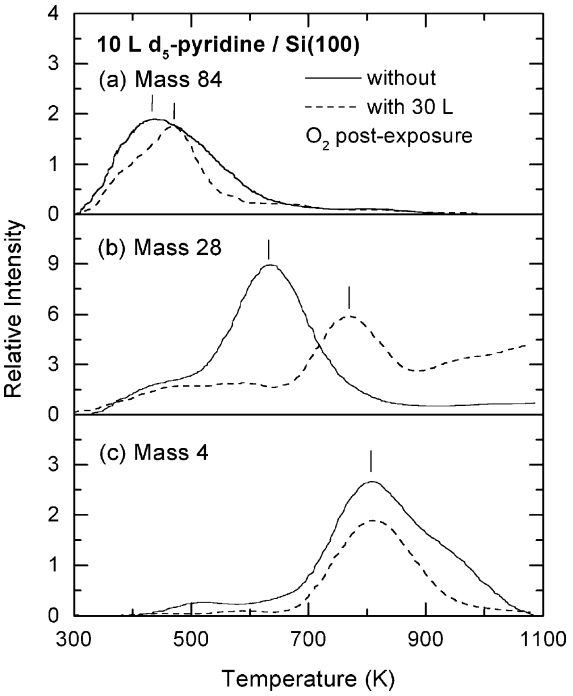

Fig. 9. Thermal desorption profiles of (a) mass 84, (b) mass 28 and (c) mass 4 for a 10 L room-temperature exposure of d_5-pyridine to Si(1 0 0)2×1 with and without a 30 L post-exposure of O_2.

the sample saturated with 10 L exposure of d_5-pyridine was post-exposed with H atoms generated from 3000 L of H_2 with a hot W filament positioned 2 cm away. To minimize the effect of radiative heating from the hot filament during the hydrogen activation, liquid nitrogen was used to keep the sample near or below RT. Fig. 10 shows rather weak (mass 84) molecular desorption, and two intense TDS features of mass 2 at 650 and 790 K, corresponding to recombinative desorption from dihydride and monohydride, respectively [39,40]. Furthermore, the desorption of mass 4 is found to be relatively weak with respect to the desorption intensities of HD (mass 3, at 20%) and H_2 (mass 2, at 10%). The shift of the D_2 (HD) TDS feature by 20 K (10 K) to a higher temperature relative to the β_1 TDS feature of H_2 (mass 2) at 790 K indicates that hydrogen evolution occurs during the thermal desorption experiment. After the RT post-exposure of H, thermally induced hydrogen

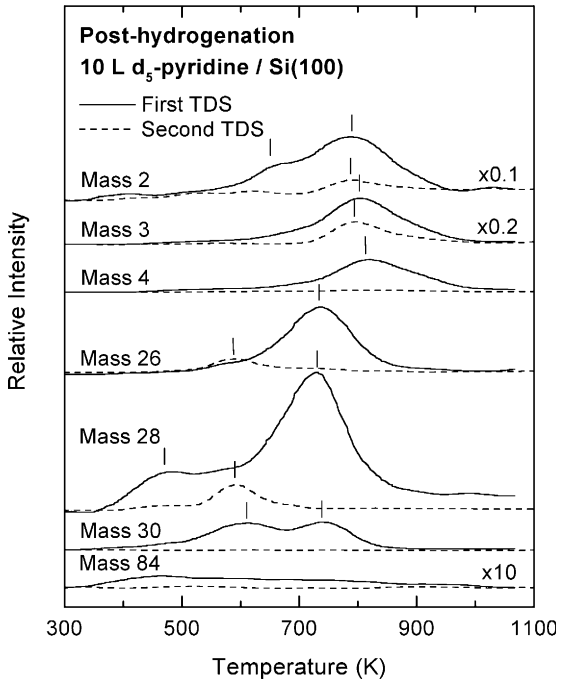

Fig. 10. Thermal desorption profiles of mass 2, 3, 4, 26, 28, 30, and 84 for a 10 L room-temperature exposure of d_5-pyridine to a Si(1 0 0)2×1 surface followed by post-exposure of hydrogen atoms. The time difference between the first and second TDS experiments was 60 min.

abstraction of the adsorbed d_5-pyridine molecules would not begin until the occupied neighboring active sites on the Si(1 0 0) surface are vacated (i.e., upon H_2 desorption). The desorption of mass 28 at 470 and 730 K, along with that of mass 26 only at 730 K, and the desorption of mass 30 at 610 and 730 K implicate rather complicated dissociation pathways possibly involving smaller hydrocarbon fragments such as $C_2D_2H_2$ [50,51]. Similar results about the adsorption and hydrogenation reactions for hexacyclic hydrocarbons (benzene, 1,3-cyclohexadiene, 1,4-cyclohexadiene, and cyclohexene) on the Si(1 0 0)2×1 surface have also been found in a combined Fourier Transform Infrared Spectroscopy and TDS study [52]. These results suggest that the C=C double bonds remaining in the chemisorbed hexacycles could react with atomic H, giving rise to a common "parent" hydrogenation product $C_5ND_5H_5$. Upon reaction with the coadsorbed H atoms during the TDS process, this hydrogenation product could dehydrogenate back to a family of hexacycles $C_5ND_mH_{n-m}$ ($m = 0$–5, $n = 5$–10) with $C_5ND_mH_{5-m}$ ($m = 0$–5) expected to be the end-products. The weak intensity observed for mass 84 (parent mass) and mass-28 intensity at 400–600 K could be attributed to the evolution of these dehydrogenated hexacycles. These dehydrogenated hexacycles could also undergo decomposition into smaller hydrocarbon fragments, including $C_2D_{4-m}H_m$ ($m = 0$–4) with plausible TDS features for masses 30, 28, and 26 at 610 K, and $C_2D_{2-m}H_m$ ($m = 0$–2) with mass-28 and mass-26 desorption at 730 K. In the case of $C_2D_{4-m}H_m$ ($m = 0$–4), the mass-30 feature at 730 K could be due to recombinative desorption of $C_2D_{2-m}H_m$ ($m = 0$–2) with surface H or D atoms likely in a highly mobile state at this temperature.

For the second TDS run, the TDS profiles for the post-hydrogenated sample shown in Fig. 10 resemble the corresponding profiles for d_5-pyridine on the H-terminated Si surface (Fig. 8). In particular, as with the H-terminated Si sample, the TDS features for mass 2, mass 4, mass 30, and mass 84 appear to have diminished significantly. Furthermore, the TDS profiles of mass 26 and mass 28 are also found to revert back to those found for the 2×1 sample (with a desorption maximum at 590 K). In contrast to the second TDS run observed for the H-terminated Si sample (Fig. 8), the TDS feature of mass 3 at 790 K for the second TDS run is found to be weaker than the first TDS run. This reduction is consistent with the hydrogenation of d_5-pyridine discussed earlier, which has the effect of diluting the relative concentration of D atoms in the resulting heterohexacycles. Because the resulting heterocycles is the main source of the D atoms for the mass-3 desorption, the reduction in the moiety of the heterocycles after the first TDS run would therefore produce less mass-3 desorption. On the other hand, in the case of H-terminated surface, hydrogenation of adsorbed d_5-pyridine appears to be unlikely (Fig. 8). The lack of unoccupied sites for the hydrogen abstraction of pyridine during the first TDS run limits the amount of mass-3 desorption while in the second TDS run the availability of newly released sites provides more hydrogen evolution opportunity, thus giving rise to a stronger mass 3 desorption (Fig. 8).

4. Conclusions

The adsorption and thermal reactions of pyridine on 2×1 and modified surfaces of Si(1 0 0) have been investigated by TDS, LEED and AES under UHV conditions. The AES results show that the second-order kinetics observed for pyridine adsorption on Si(1 0 0)2×1 is consistent with a more complicated process (relative to benzene) possibly involving hydrogen abstraction and/or fragmentation at RT. Furthermore, the saturation coverage of pyridine on Si(1 0 0)2×1 is found to be 0.41 ML, corresponding to two pyridine molecules for every three Si dimers, which is higher than that of benzene (0.27 ML [18], with one benzene molecule for every two Si dimers). The (2×1) LEED pattern obtained after adsorption indicates that the overall structure of the reconstructed Si(1 0 0) surface is not significantly affected by the chemisorption of pyridine at RT. However, pyridine is found to undergo several competitive thermal reactions on Si(1 0 0)2×1, involving the N-end-on atop and di-σ bonded cycloaddition states. The 1,4 and 2,5 di-σ adsorption states are believed to give rise to molecular desorption while the more stable N-end-on atop adsorption state could be responsible for the dissociation pathways such as hydrogen abstraction and fragmentation.

Unlike the results in our previous study of pyridine on Si(1 1 1)7×7, where rapid dissociation of adsorbed pyridine upon irradiated by low-energy electrons at RT was observed [14], pyridine was found for the first time to undergo condensation oligomerization on Si(1 0 0)2×1 mediated by low-energy electrons. This result is significant in providing a viable method for imprinting a highly "crystalline" polymer prealigned by the surface template onto a pattern generated by an electron beam writer (in a way similar to electron beam lithography). Furthermore, similar oligomerization has also been observed for an oxidized Si surface without low-energy electron mediation. These observations are supported by the shift in temperature of the desorption maximum of the TDS feature for hydrogen evolution and by a distinct molecular desorption in the second TDS run. The present work also illustrates that "repeated" TDS runs could be very useful for elucidating the consequence of surface processes upon thermal excitation and desorption.

Various thermal reactions, including molecular, dissociative and associative desorption, hydrogen abstraction, fragmentation, and oligomerization as well as oxidization, involving different adsorption states could be inferred from the coordinated evolution of hydrogen and higher fragments in the TDS profiles. As shown in the present work, these reactions have been further studied under different surface conditions, and with various pre- and post-treatments (including oxidation, hydrogenation, and low-energy electron mediation). In contrast to benzene, which was found to adsorb and desorb molecularly, pyridine evidently exhibits a more active surface chemistry on Si(1 0 0)2×1 likely due to the presence of the lone-pair electrons on the N heteroatom. It may therefore be feasible to manipulate and control the outcome of different surface processes by changing the heteroatom in the case of heterocyclic silicon surface chemistry. More detailed ab initio calculations and other experimental investigations using different surface analysis techniques (such as variable-temperature scanning probe microscopy) will be of great interest to further elucidate the intricate adsorption geometries and mechanisms as well as the surface reactions (with and without electron mediation) of these important heterocyclic hydrocarbons on Si(1 0 0).

Acknowledgement

This work was supported by the Natural Sciences and Engineering Research Council of Canada.

References

[1] A. Tsumura, H. Koezuka, T. Ando, Appl. Phys. Lett. 49 (1986) 1210.
[2] A. Garito, R.F. Shi, M. Wu, Phys. Today 47 (1994) 51.
[3] J.R. Ostrick, A. Dodabalapur, L. Torsi, A.J. Lovinger, E.W. Kwock, T.M. Miller, M. Galvin, M. Berggren, H.E. Katz, J. Appl. Phys. 81 (1997) 6804.
[4] V.I. Krinichnuyi, Phys. Solid State 39 (1997) 1.
[5] T.A. Skotheim, R.L. Elsenbaumer, J.R. Reynolds (Eds.), Handbook of Conducting Polymers, Dekker, New York, 1998.

[6] K.M. Baumgartner, M. Volmer-Uebing, J. Taborski, P. Bauerle, E. Umbach, Ber. Bunsen-Ges. Phys. Chem. 95 (1991) 1488.
[7] H.N. Waltenburg, J.T. Yates, Chem. Rev. 95 (1995) 1589.
[8] R.J. Hamers, Y. Wang, Chem. Rev. 96 (1996) 1261.
[9] R.J. Hamers, J.S. Hovis, C.M. Greenlief, D.F. Padowitz, Jpn. J. Appl. Phys. 38 (1999) 3879.
[10] J.T. Yates Jr., Science 279 (1998) 335.
[11] D.R. Lide (Ed.), CRC Handbook of Chemistry and Physics, CRC Press LLC, Cleveland, 2001.
[12] M.N. Piancastelli, G. Margaritondo, J.E. Rowe, Solid State Commun. 45 (1983) 219.
[13] M.N. Piancastelli, M.K. Kelly, G. Margaritondo, J. Anderson, D.J. Frankel, G.J. Lapeyre, Phys. Rev. B 32 (1985) 2351.
[14] C.D. MacPherson, K.T. Leung, Surf. Sci. 324 (1995) 202.
[15] S. Yagi, N. Shirota, M. Taniguchi, E. Hashimoto, Surf. Sci. 454–456 (2000) 157;
N. Shirota, S. Yagi, M. Taniguchi, E. Hashimoto, J. Vac. Sci. Technol. A 18 (2000) 2578.
[16] X. Lu, X. Xu, J. Wu, N. Wang, Q. Zhang, New J. Chem. 26 (2002) 160.
[17] X. Lu, M.C. Lin, X. Xu, N. Wang, Q. Zhang, Phys. Chem. Commun. 13 (2001) 1.
[18] Y. Taguchi, M. Fujisawa, T. Takaoka, T. Okada, M. Nishijima, J. Chem. Phys. 95 (1991) 6870.
[19] Y. Taguchi, Y. Ohta, T. Katsumi, K. Ichikawa, O. Aita, J. Electron Spectrosc. Relat. Phenom. 88–91 (1998) 671.
[20] S. Gokhale, P. Trischberger, D. Menzel, W. Widdra, H. Droge, H.-P. Steinruck, U. Birkenheuer, U. Gutdeutsch, N. Rosch, J. Chem. Phys. 108 (1998) 5554.
[21] M.J. Kong, A.V. Teplyakov, J.G. Lyubovitsky, S.F. Bent, Surf. Sci. 411 (1998) 286.
[22] G.P. Lopinski, D.J. Moffatt, R.A. Wolkow, Chem. Phys. Lett. 282 (1998) 305.
[23] G.P. Lopinski, T.M. Fortier, D.J. Moffatt, R.A. Wolkow, J. Vac. Sci. Technol. A 16 (1998) 1037.
[24] B. Borovsky, M. Krueger, E. Ganz, Phys. Rev. B 57 (1998) R4269.
[25] B.I. Craig, Surf. Sci. 280 (1993) L279.
[26] H.D. Jeong, S. Ryu, Y.S. Lee, S. Kim, Surf. Sci. 344 (1995) L1226.
[27] U. Birkenheuer, U. Gutdeutsch, N. Rosch, Surf. Sci. 409 (1998) 213.
[28] R.A. Wolkow, G.P. Lopinski, D.J. Moffatt, Surf. Sci. 416 (1998) L1107.
[29] P.L. Silvestrelli, F. Ancilotto, F. Toigo, Phys. Rev. B 62 (2000) 1596.
[30] B. Borovsky, M. Krueger, E. Ganz, J. Vac. Sci. Technol. B 17 (1999) 7.
[31] Q. Li, K.T. Leung, Surf. Sci. 479 (2001) 69.
[32] Texas Instruments TMS320C5X DSP Starter Kit User's Guide, Microprocessor Development Systems, Texas Instruments Inc., 1994.
[33] W. Kern, D.A. Puotinen, RCA Rev. 31 (1970) 187.
[34] Q. Li, Ph.D. dissertation, University of Waterloo, Waterloo, 2003.
[35] NIST/EPA/NIH Mass Spectral Library, NIST'98 with Windows, Version 1.7, 1996.
[36] P.A. Redhead, Vacuum 12 (1962) 203.
[37] M.J. Frisch et al., Gaussian 98 (Revision A.11.3), Gaussian Inc., Pittsburgh, PA, 2002.
[38] J.B. Foresman, Æ Frisch, Exploring Chemistry with Electronic Structure Methods, second ed., Gaussian Inc., Pittsburgh, 1996, and references therein.
[39] M. Suemitsu, H. Nakazawa, N. Miyamoto, Appl. Surf. Sci. 82/83 (1994) 449.
[40] S.M. Gates, R.R. Kunz, C.M. Greenlief, Surf. Sci. 207 (1989) 364.
[41] P.A. Taylor, R.M. Wallace, C.C. Cheng, W.H. Weinberg, M.J. Dresser, W.J. Choyke, J.T. Yates Jr., J. Am. Chem. Soc. 114 (1992) 6754.
[42] C. Huang, W. Widdra, X.S. Wang, W.H. Weinberg, J. Vac. Sci. Technol. A 11 (1993) 2250.
[43] V.N. Ageev, Prog. Surf. Sci. 47 (1994) 55, and references therein.
[44] L. Clemen, R.M. Wallace, P.A. Taylor, M.J. Dresser, W.J. Choyke, W.H. Weinberg, J.T. Yates Jr., Surf. Sci. 268 (1992) 205.
[45] C.C. Cheng, W.J. Choyke, J.T. Yates Jr., Surf. Sci. 231 (1990) 289.
[46] N.M. Marinov, W.J. Pitz, C.K. Westbrook, M.J. Castaldi, S.M. Senkan, Combust. Sci. Technol. 116–117 (1996) 211, and references therein.
[47] S.J. White, D.P. Woodruff, B.W. Holland, R.S. Zimmer, Surf. Sci. 74 (1978) 34.
[48] Y. Imamura, N. Matsui, Y. Morikawa, M. Hada, T. Kubo, M. Nishijima, H. Nakatsuji, Chem. Phys. Lett. 287 (1998) 131.
[49] R.Y. Young, K.A. Brown, W. Ho, Surf. Sci. 336 (1995) 85.
[50] L.H. Chua, R.B. Jackman, J.S. Foord, Surf. Sci. 315 (1994) 69.
[51] W. Widdra, C. Huang, S.I. Yi, W.H. Weinberg, J. Chem. Phys. 105 (1996) 5605.
[52] M.J. Kong, A.V. Teplyakov, J. Jagmohan, J.G. Lyubovitsky, C. Mui, S.F. Bent, J. Phys. Chem. B 104 (2000) 3000.